Energy Transfer between CdZnS Quantum Dots and Perylene Diimide Dyes

Na Wu,[a,b] Nicholas Kirkwood,[a] Nicolau Saker Neto,[a] Rehana Pervin,[a] Paul Mulvaney,[a] Wallace W. H. Wong.[a]*

[a] ARC Centre of Excellence in Exciton Science, School of Chemistry, University of Melbourne, Parkville, VIC., 3010, Australia.

[b] Suzhou Institute of Nano-Tech and Nano-Bionics, Chinese Academy of Sciences, Suzhou, China.

*Email: wwhwong@unimelb.edu.au

Abstract

QD-dye systems are promising models for artificial photosynthesis and down converter systems for LEDs and displays. To better understand the factors controlling energy transfer from the QDs to the dyes, we fabricated a series of $Cd_xZn_{1-x}S/ZnS$ quantum dot (QD)-perylene diimide (PDI) composite nanocrystals. The core-shell $Cd_xZn_{1-x}S/ZnS$ QDs were chosen for better control of surface chemistry and for control of photophysical properties through core composition. The PDIs were designed with bulky substituents to reduce dye-dye aggregation effects. Energy transfer efficiency was found to depend upon both the length of the anchoring alkyl chain and the type of terminal anchoring group. The maximum energy transfer efficiency of 91% from QDs to PDIs was achieved with composites containing PDIs with carboxylic acid anchoring groups and longer alkyl chains. It was found that composites with carboxylic acid anchors exhibited greater photostability than composites with amine anchors. Longer alkyl chains also led to greater photostability. Conversely, shorter chain alkanes promoted faster aggregation of the nanocrystal composites.

Introduction

Hybrid organic-inorganic nanoparticle systems consisting of semiconductor quantum dots (QDs) and functionalized organic materials are of great interest for application in various fields including energy conversion, optoelectronics, imaging, and sensing.[1-9] Colloidal QDs are semiconductor nanocrystals with size-, shape-, and composition-dependent optoelectronic properties. Conventionally, simple surfactants have been used to disperse the QDs in solvents of various polarity. However, exchange of the native surface ligands with other functional molecules can be used to impart new chemical properties, such as biocompatibility or to enhance their electrical conductivity in optoelectronic devices.[10-13] The properties of organic dyes can be finely tuned by even single atom exchange of their molecular structure. By combining QDs and organic fluorophores, the resulting hybrid materials have unique optical properties and are of great interest for spectral engineering in various fields.[4]

Energy transfer between QDs and organic dyes in hybrid systems generally obeys a $1/d^6$ distance-dependence, because of Förster resonance energy transfer (FRET).[6, 14-15] FRET occurs via a dipole-dipole coupling mechanism for energy transfer between an excited state energy donor (D) and a ground state energy acceptor (A). Such energy transfer requires spectral overlap of the donor emission with the absorption spectrum of the acceptor, small separations between the donor and acceptor (1-10 nm), and favorable orientation of the molecular transition dipole moments.

Perylene diimide dyes (PDI) are a relatively photostable class of luminescent dye with tunable absorption spectra and high fluorescence quantum yields. They can be easily derivatized with long chain anchor groups and they exhibit good solubility in a wide range of solvents. Because multiple acceptors can bind to a single QD, more efficient energy transfer is possible.[16] The hybrid system can exhibit increased Stokes shift and there may even be an increase in the overall photoluminescence quantum yield (Φ_{PL}) if FRET can compete with radiation-less relaxation pathways in the QD. The properties of these composite hybrids can be readily tuned by controlling the QD size, shape, and composition, and by varying the chemical structures of the acceptor dyes.

The PDI acceptors may be bound to the nanocrystals or remain as free molecules in solution.[17] Due to the short range of the FRET process, only the adsorbed acceptor molecules are likely to participate in energy transfer. The PDI molecules may both adsorb and desorb from the nanocrystal. This dynamic adsorption equilibrium can affect both the quenching efficiency as well as the colloidal stability of the QDs in solution. The mechanism of ligand exchange has been investigated using nuclear magnetic resonance (NMR) and luminescence spectroscopy.[18-20] In particular, the binding of alkylamines has been shown to be a dynamic process with a rapid exchange between the bound and free state on the QD surface; this lability has been observed in CdSe,[18] CdTe,[21] PbS,[22] and ZnO QDs.[21, 23] Energy transfer and ligand exchange mechanisms have often been investigated separately. For

example, Dworak et al. investigated the acceptor concentration dependence of FRET dynamics in QD-dye complexes by steady state and time-resolved spectroscopy.[24] Liu et al. studied the ligand exchange mechanism with alkylamines on the surface of CdSe QDs by using ^{1}H NMR spectra.[17] FRET has also been used to study ligand exchange kinetics on a CdS/bodipy dye system[25] in which ligands were shown to bind to distinct sites on the QD surface modulating energy and charge transfer.[26] In this work, we investigated both the nanocrystal stability and energy transfer for a series of QD-PDI nanocrystals with the aim to maximize energy transfer efficiency and emission output. We chose core-shell $Cd_xZn_{1-x}S$/ZnS QDs to minimize the influence of surface defects[27] with $Cd_xZn_{1-x}S$ cores to adjust the photophysical properties of the QDs by composition rather than size.[28] The PDIs were also specifically designed with bulky substituents to reduce the effect of dye-dye aggregation on the QD surface as these aggregates often lead to non-emissive states. By varying the ligand chain length and the nature of the anchoring group, a maximum energy transfer efficiency of 91% and photoluminescence quantum yield of 57% were observed.

Experimental section

Materials

$Cd_xZn_{1-x}S$/ZnS QDs were synthesized following literature procedures (see Supporting Information).[28] A highly reactive sulfur 1-octadecene (S-ODE) solution was injected twice into a mixture of $Cd(OA)_2$ and $Zn(OA)_2$ at a high temperature (310 ^{o}C) to form the alloyed $Cd_xZn_{1-x}S$ core and ZnS shell. The composition of the $Cd_xZn_{1-x}S$ core was tuned by adjusting the amount of sulfur in the reaction. The $Cd_xZn_{1-x}S$ /ZnS QDs were capped by an oleate layer with carboxylate groups binding the surfactant to the QD surface. From TEM analysis (Figure S1), the $Cd_xZn_{1-x}S$ /ZnS QDs had a nearly spherical shape with size distribution of 8.5 ± 1.9 nm. The chemical composition of the $Cd_xZn_{1-x}S$ /ZnS QDs was measured by inductively coupled plasma optical emission spectroscopy (ICP-OES) with the quantification of Cd^{2+} and Zn^{2+} in digested samples at different concentrations (see the Supporting information). The molar ratio of Cd^{2+} to Zn^{2+} in the final QDs was found to be 1:1.

The four PDI derivatives, PDI-C4-NH_2, PDI-C12-NH_2, PDI-C5-COOH, and PDI-C11-COOH, were synthesized in 5 steps from commercial starting materials. Briefly, perylene dianhydride was esterified to give perylene tetracarboxylic acid butyl ester followed by mono-imidization with 2,5-dibromoaniline. The bulky di-*tert*-butylphenyl groups were installed by Suzuki-Miyaura coupling and, finally, the anchoring chains were attached via a second imidization over two steps. Detailed synthesis procedures are described in the Supporting information. The PDIs were characterized by NMR and mass spectroscopy with details provided in the Supporting information.

QD-PDI hybrid nanocrystals

In a typical ligand exchange process, 3 mg/mL $Cd_xZn_{1-x}S$ /ZnS QDs solution were mixed with functionalized PDI dyes at various concentrations (2×10^{-5} M, 5×10^{-5} M, 7×10^{-5} M, 1×10^{-4} M, 2×10^{-4} M, 5×10^{-4} M, 7×10^{-4} M,) in $CHCl_3$. The molar concentration of $Cd_xZn_{1-x}S$ /ZnS QDs was 2.33×10^{-6} M calculated from ICP-OES and the optical extinction coefficients. Thus, the molar ratios of QDs to PDI dyes in the ligand exchange solutions were 1:9, 1:21, 1:30, 1:43, 1:86, 1:215 and 1:300. The mixtures were stirred overnight at room temperature to afford QD-PDI nanocrystals in solution. Then the solutions were washed with acetone to remove any free PDI dye. The supernatant and precipitates were separated by centrifuge (6600 rpm, 5 min). The composite nanocrystals were then further purified by redispersion-precipitation (3 iterations) with chloroform/acetone using the same centrifuge speed. The QD-PDI nanocrystals were then dispersed in chloroform for photophysical characterization.

Optical spectroscopy measurement

UV-Vis absorbance spectra were measured by Agilent HP8453 UV-Vis spectrophotometer. The fluorescence emission spectra of all samples were recorded by a Horiba Jobin Yvon FluorologOR -3 fluorometer at excitation wavelength of 365 nm (excitation slit width 1 nm, emission slit width 1 nm, integration time 0.1 s). The fluorescence excitation wavelength of all PDI-based samples were detected with the emission at 620 nm (excitation slit width 1 nm, emission slit width 1 nm, integration time 0.1 s). Absolute photoluminescence quantum yield (Φ_{PL}) of all samples was measured by using integrated sphere (F3018, Horiba Jobin Yvon) on the FluorologOR -3 fluorometer. All spectra for the absolute quantum yield measurements were corrected for the light source noise, wavelength sensitivity and the transmittance of filters. The time correlated single photon counting was measured by Deltaflex-Horiba JobinYvon time correlated single photon counting system. These samples were excited at 300 nm using nanosecond diode lasers with the repetition of 1 MHz. The fluorescence decays are analysed by DSA 6 software from the above-mentioned instrument.

Results and discussion

In Figure 1, we show the structures of the various PDI dyes and the absorption and emission spectra of both the dyes and the CdSe/ZnS nanocrystals. Di-*tert*-butylphenyl substituents were positioned around the imide functionalities of the PDI core to reduce the likelihood of intermolecular π-π stacking of the PDI compounds.[29] This design was implemented to reduce aggregation-induced quenching (AIQ) of PDI photoluminescence when the chromophores were anchored on the QD surface. The PDIs were functionalized with either terminal amine or carboxylic acid groups, while

the distance between the QDs and the PDI chromophores was adjusted by varying the anchoring group alky chain length. Shorter alkyl chains (4 and 5 carbons) and longer alkyl chains (11 and 12 carbons) were chosen (Figure 1), and the corresponding PDI derivatives were named PDI-C4-NH_2, PDI-C12-NH_2, PDI-C5-COOH, and PDI-C11-COOH.

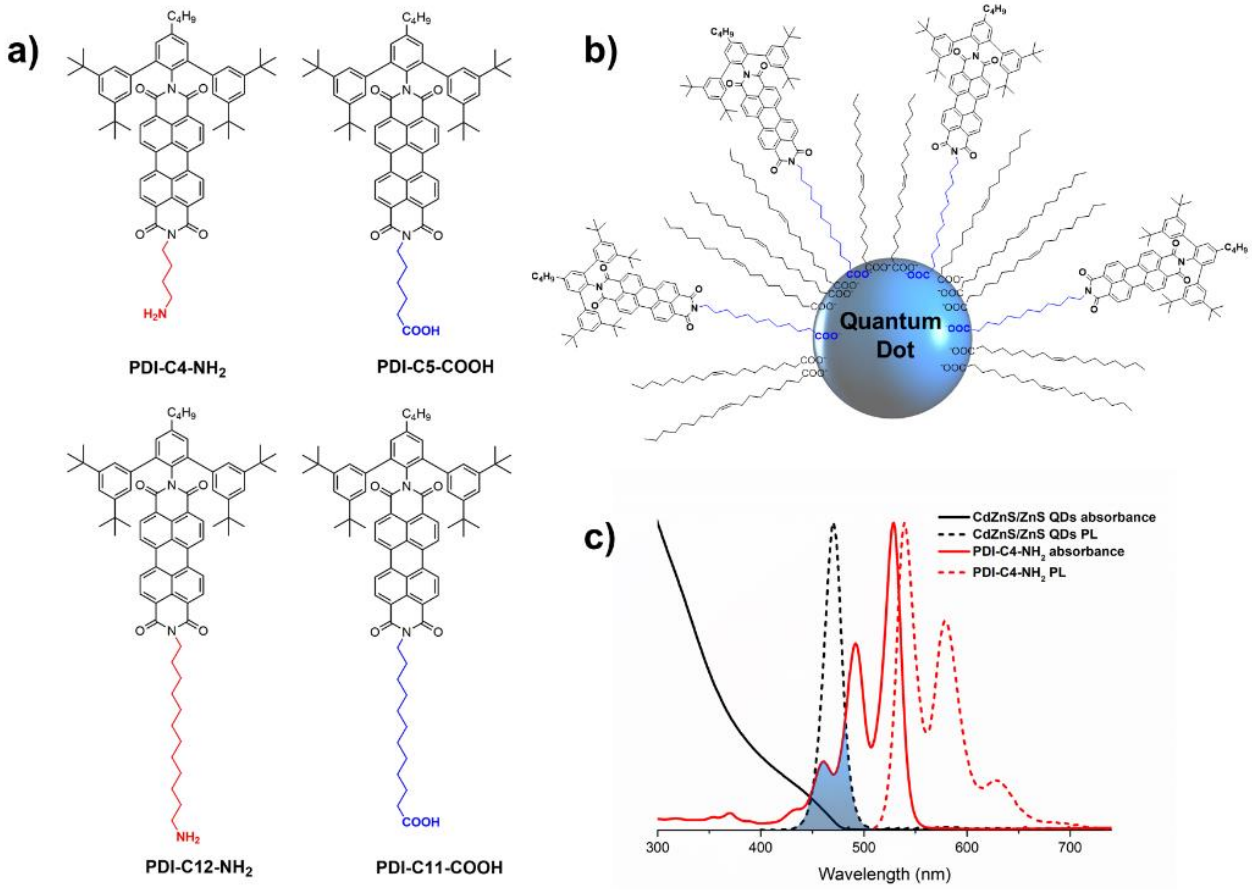

Figure 1. a) The chemical structure of functionalized PDI derivatives and b) the schematic graph of $Cd_xZn_{1-x}S$/ZnS QD-PDI-C11-COOH composite. c) The normalized absorbance and PL spectra of $Cd_xZn_{1-x}S$/ZnS QDs and PDI-C4-NH_2 in $CHCl_3$ solution. $Cd_xZn_{1-x}S$/ZnS QDs were excited at 365 nm. PDI-C4-NH_2 were excited at 490 nm. The filled blue area denotes the spectral overlap between the QD PL and the PDI-C4-NH_2 absorbance spectrum. Chloroform was used as the solvent.

Photophysical properties of PDI derivatives. The UV-Vis absorbance spectra of the various PDI compounds in dilute solution (1×10^{-5} M) were identical to each other. They displayed three absorption bands with peaks at 459, 492, and 528 nm, with the typical PDI fine structure (Figure S2a, Table S1). The PL spectra of the PDI compounds were collected following excitation at 490 nm, and these were also similar, exhibiting emission peaks at 538, 577, and 625 nm. The time resolved PL emission exhibited a clean, single exponential decay curve which indicated there was one dominant photo-excited species in each sample (Figure S2c). The fluorescence lifetime of the emission at 538 nm was around 4 ns. The absolute Φ_{PL} of all the PDI compounds was close to 90% in chloroform. These values were determined via measurements in an integrating sphere. As expected, the different

imide substituents in these compounds did not affect the photophysical properties. It was previously reported that PDI compounds with a bulky di-*tert*-butylphenyl substituent (as used in this study) exhibited a higher concentration tolerance of AIQ effect than the corresponding PDI without bulky substituent.[22] We used the same bulky substituent on one of the imides of the PDI to reduce PDI aggregation at high concentration. This was important as the local concentration of PDIs on the QD surface was expected to be high. As shown in the normalized PL spectra of PDI-C5-COOH solution (Figure S2b), the PL peak at 538 nm red-shifted and its relative intensity decreased with increased concentration from 1×10^{-6} M to 1×10^{-3} M. There was no obvious change in the PL peaks at 577 nm and 625 nm, and these did not exhibit the typical broadened PL peak that occurs upon aggregation. The change in PL spectra in concentrated solutions of PDIs was attributed to re-absorption, due to the small Stokes shift in these molecules. Thus, these amine or carboxylic acid functionalized PDI derivatives showed little aggregation up to 1×10^{-3} M.

Photophysical properties of $Cd_xZn_{1-x}S/ZnS$ QDs. To match the emission of the QDs to the absorption spectra of the PDIs, blue-emitting ternary alloyed $Cd_xZn_{1-x}S$ core QDs with a ZnS shell were introduced as the energy donor to harvest UV light. The core-shell structure was grown to remove surface defects and improve Φ_{PL}.[27] The UV-Vis absorbance spectra of these QDs are shown in Figure 1c revealing an absorbance edge at 481 nm. The PL peak of $Cd_xZn_{1-x}S/ZnS$ QDs was located at 471 nm with a full width at half maximum (FWHM) of 18 nm and absolute Φ_{PL} of 45% in $CHCl_3$ solution. The molar extinction coefficient of $Cd_xZn_{1-x}S/ZnS$ QDs was determined to be 5.30×10^6 M^{-1} cm^{-1} in $CHCl_3$ solution at 365 nm. This value was obtained by determining the molar concentration of the sample from the estimated weight of each QD. QD density, estimated from ICP-OES data, and the average QD size from TEM analysis gave the estimated QD particle weight (see Supporting Information file for details). The PL spectrum of the QDs and the absorbance spectrum of PDI-C4-NH_2 are shown in Figure 1c, demonstrating they are well-suited to FRET experiments.

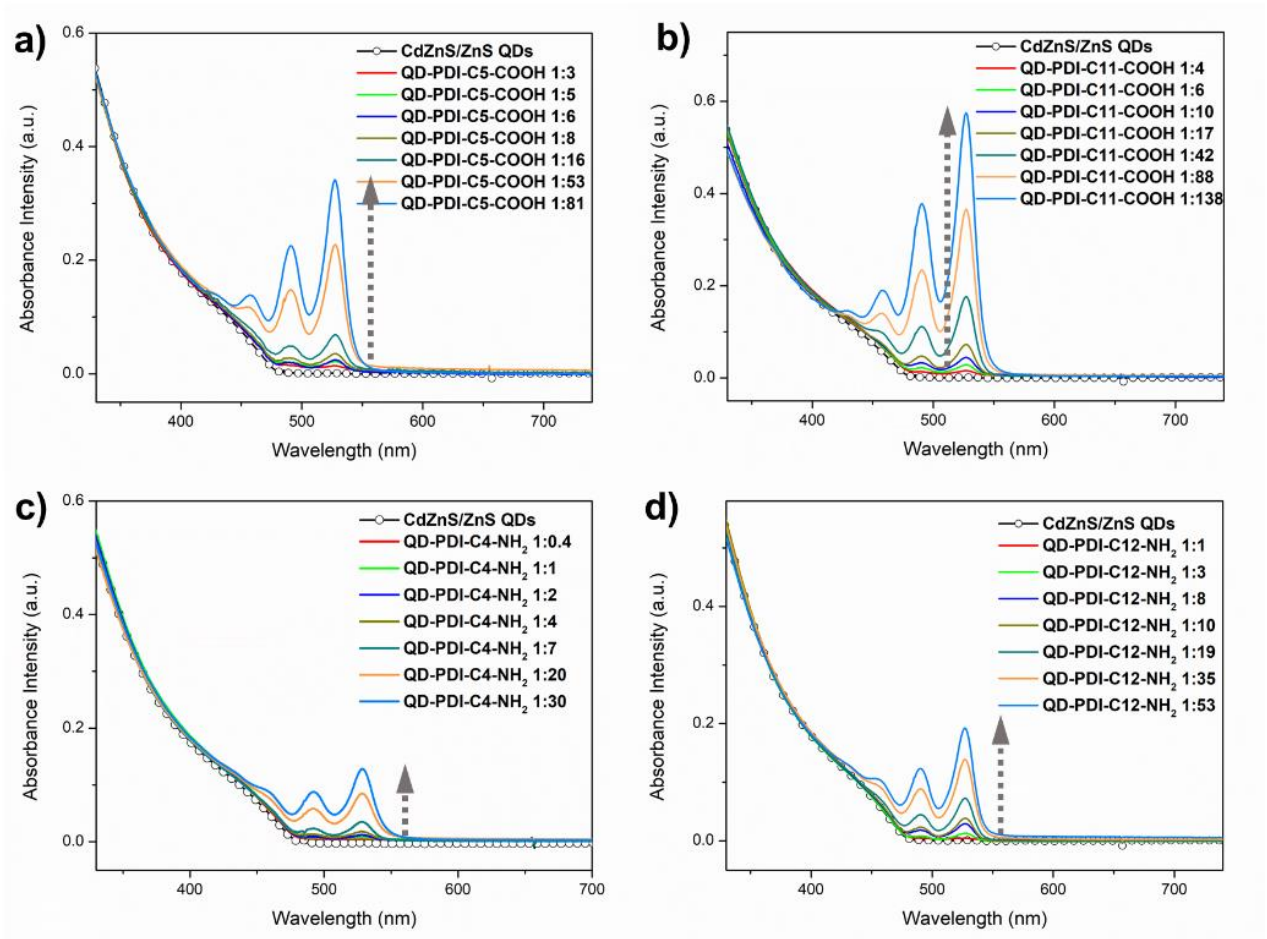

Figure 2. The absorbance spectra of QD-PDI hybrid nanocrystals in $CHCl_3$ solution with different PDI ratios. a) QD-PDI-C5-COOH composites, b) QD-PDI-C11-COOH composites, c) QD-PDI-C4-NH_2 composites, and d) QD-PDI-C12-NH_2 composites.

QD-PDI hybrid nanocrystals. The QD-PDI composites were prepared by ligand exchange of the oleate ligands with the PDI derivatives (see experimental section for details). By increasing the PDI concentration, the molar ratio of QDs to PDI in the composite NCs could be varied is evident from the increase in PDI absorbance (Figure 2). The final ratios of $Cd_xZn_{1-x}S$/ZnS QDs to PDI in the hybrid NCs were calculated after purification of the composites, from the absorbance at 365 nm and 528 nm, respectively, using their molar extinction coefficients.

In the ligand exchange reactions, the initial concentrations of the different PDIs were the same in these four sets of reactions. However, due to the different anchoring groups and alkyl chain lengths of the PDIs, the final QD:PDI ratios in the NCs differed significantly (Figure 2, Table 1). The QD-PDI-C11-COOH nanocrystals achieved the highest PDI binding ratio of 1:138 (from an initial solution phase ratio of 1:300). This is attributed to two structural features of the PDI derivative. The longer alkyl chain enabled the PDI-C11-COOH molecules to penetrate the dense native oleate layer efficaciously and the carboxylic acid group results in stronger bonding to the QD surface compared

amine anchor groups (Figure 1b). The shorter chain molecule PDI-C5-COOH exhibited a lower binding affinity to the QD surface. In general, PDIs with carboxyl groups had higher affinity than those with amine functionalities. For example, PDI-C4-NH_2 and PDI-C12-NH_2 exhibited lower adsorption densities than PDI-C5-COOH and PDI-C11-COOH, respectively. PDI-C4-NH_2 had the lowest binding affinity of the four PDIs studied.

From the ICP-OES and UV-Vis spectroscopy results, the coverage of PDIs and oleates on the QD surface could be quantified. In the as-synthesized $Cd_xZn_{1-x}S/ZnS$ QDs, the coverage of oleate ligands on the QD surface calculated from the mass of oleate and the average surface area per QD, was 6 oleates /nm^2. In QD-PDI composites, the highest surface anchoring densities were found to be: 0.35 PDI-C5-COOH /nm^2, 0.60 PDI-C11-COOH /nm^2, 0.13 PDI-C4-NH_2 /nm^2, and 0.23 PDI-C12-NH_2 /nm^2. Hence the majority of oleate ligands remained bound to the QD-PDI composites. Unfortunately, the surface density of oleate ligands in the hybrid nanocrystals could not be quantified by ^{1}H NMR experiments directly due to the overlap of the oleate and PDI NMR spectra. The estimated densities of the PDI dyes on the QD surface can be converted to average distances between PDI molecules bound on the QD surface which are 0.65 nm, 0.40 nm, 0.87 nm, and 0.77 nm for PDI-C5-COOH, PDI-C11-COOH, PDI-C4-NH_2 and PDI-C12-NH_2, respectively. Since the PDI chromophore is quite bulky with size around 1 nm^2, PDI to PDI interactions on the QD surface are likely to be observed (see later discussion on PDI aggregation).

Tables 1. The adsorbed molar ratio QDs:PDI in composite nanocrystals as a function of the initial PDI ratios in the ligand exchange solution.

ligand exchange molar ratio (QD: PDI)	QD-PDI-C5-COOH	QD-PDI-C11-COOH	QD-PDI-C4-NH_2	QD-PDI-C12-NH_2
1:9	1:3	1:4	1:0.4	1:1
1:21	1:5	1:6	1:1	1:3
1:30	1:6	1:10	1:2	1:8
1:43	1:8	1:17	1:4	1:10
1:86	1:16	1:42	1:7	1:19
1:215	1:53	1:88	1:20	1:35
1:300	1:81	1:138	1:30	1:53

FRET Measurements

According to the FRET theory for energy transfer,[6] the critical FRET distance R_0 (which is the molecular distance where the efficiency of FRET is 50%) is given by Equation 1:

$$R_0 = \left[\frac{9(\ln 10)\kappa^2 \Phi_D}{128\pi^5 N_{Av} n^4} J\right]^{1/6} \quad (1)$$

while the spectral overlap integral J in the QD-PDI system is given by:

$$J = \int I_D \varepsilon_A \lambda^4 \, d\lambda \quad (2)$$

where Φ_D is the photoluminescence quantum yield of the donor, N_{Av} is Avogadro's number, n is the refractive index of the medium (n = 1.446 for $CHCl_3$ solution was used in the calculations. It is also possible to use the refractive index of the oleate ligand layer, n = 1.459, as the FRET medium but this would have made little difference since the refractive index values of $CHCl_3$ and oleate are similar), κ^2 is the orientation factor between the donor and acceptor (κ^2 = 2/3 for random orientation. This is a reasonable assumption since the alkyl dye linkers are highly flexible), I_D is the normalized fluorescence intensity of the donor, ε_A is the extinction coefficient of the acceptor, and λ is the wavelength in vacuo. The values of R_0 and J in the QD-PDI systems were calculated from Equations 1 and 2 with the values listed in Table S1.

The PL emission spectra for QD-PDI samples are presented in Figure 3 following excitation at 365 nm. As is evident, the PL intensity of QDs at the emission peak of 471 nm was significantly quenched as the concentration of adsorbed PDIs was increased. There was 95%, 93%, 93%, and 86%, quenching of the QD PL at the highest PDI loading ratios, for the hybrid nanocrystal composites: QD-PDI-C5-COOH (QD:PDI, 1:81), QD-PDI-C11-COOH (1:138), QD-PDI-C4-NH_2 (1:30), and QD-PDI-C12-NH_2 (1:53), respectively. It was worth noting that there was 83% quenching for PDI-C5-COOH (1:16), while QD-PDI-C11-COOH (1:17) composites exhibited 80% quenching (Figure 3a, b). The quenching efficiency was lower for longer donor-acceptor distances at similar QD:PDI ratios. Similarly, the quenching of the QD PL in QD-PDI-C12-NH_2 composites was less efficient than in QD-PDI-C4-NH_2 composites, e.g., there was 93% and 81% quenching in QD-PDI-C4-NH_2 (1:30) and QD-PDI-C12-NH_2 (1:35) nanocrystals (Figure 3a, b), respectively. These results all demonstrate that PDI is an efficient quencher of QD luminescence, and that the efficiency depends on the PDI surface loading.

Due to the bulky structure of PDIs, more surface area is required to bind PDIs than native oleate ligands. The PDI derivatives with longer alkyl chains achieved better surface ligand coverage because of their better penetration of the oleate ligand shell. However, due to the larger donor-acceptor distance, they exhibited less efficient PL quenching.

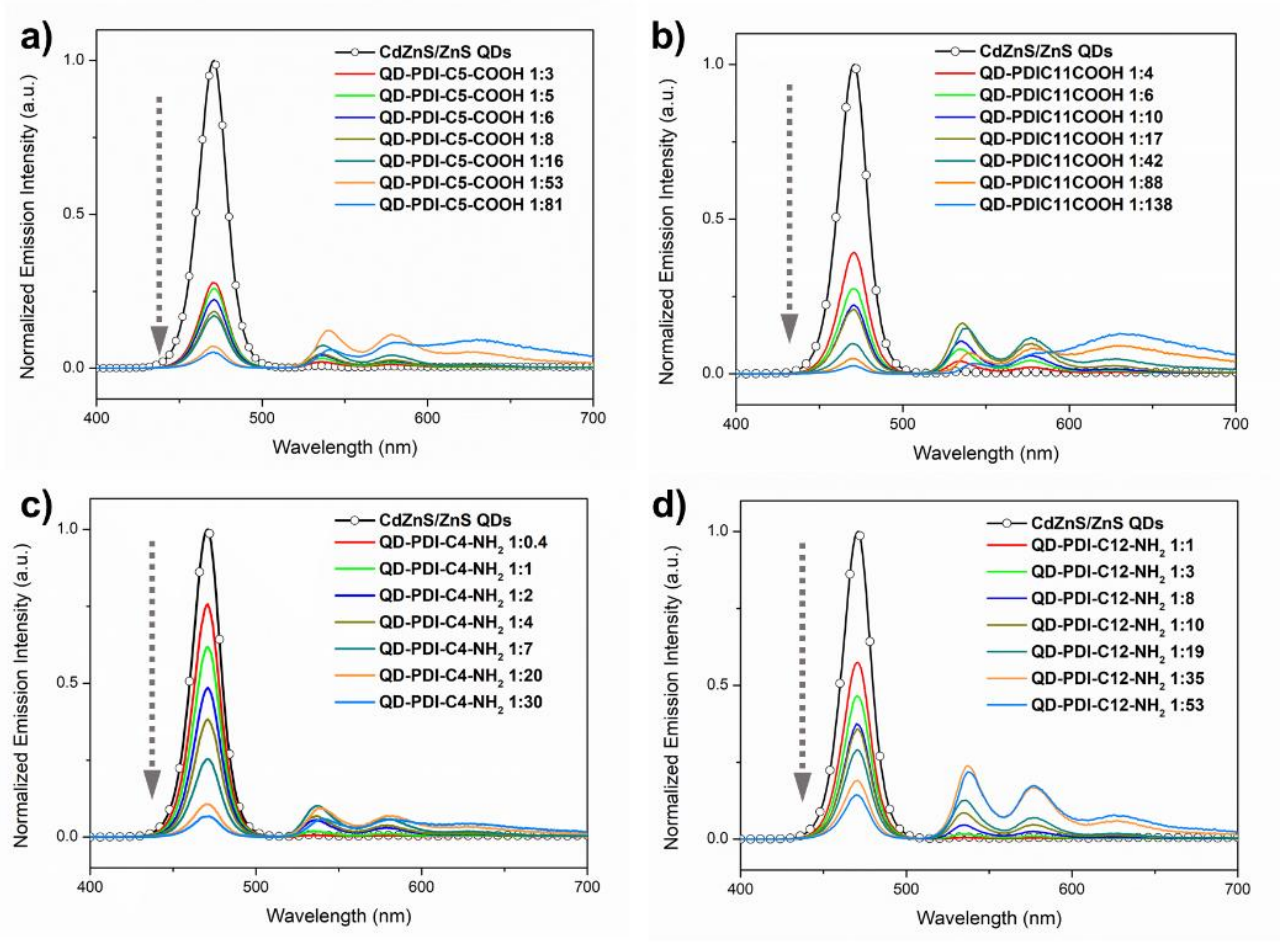

Figure 3. The PL spectra of QD-PDI composites in $CHCl_3$ solution. a) QD-PDI-C5-COOH composites, b) QD-PDI-C11-COOH composites, c) QD-PDI-C4-NH_2 composites, and d) QD-PDI-C12-NH_2 composites. All samples were excited at 365 nm. The emission peak of QDs was at 471 nm. The PDI emission peaks ranging from 520 to 700 nm are typical of PDI monomers, but they do exhibit red-shifted aggregate emission as well.

Assuming that the quenching is due to dipole coupling, the FRET efficiency can be calculated from the change in either the PL intensity (I) or fluorescence lifetime (τ) of QDs in the composite nanocrystals relative to that of the QDs in the absence of PDI dyes (I_0 or τ_0, respectively):

$$E_{FRET} = 1 - \frac{I}{I_0} = 1 - \frac{\tau}{\tau_0} \qquad (3)$$

However, PL quenching may also be due to QD surface defects created by PDI-oleate exchange reactions. Therefore, excitation spectra of the composite samples were collected to calculate the FRET efficiency (E_{FRET}). [33] The FRET process results in an increase in the PDI emission in the presence of the QD. E_{FRET} can be obtained from the excitation spectrum and the extinction spectrum of the system using the following equation:

$$A = \chi_{PDI} + E_{FRET}\chi_{QD} \qquad (4)$$

where A is the normalized extinction spectrum (normalized to the PDI peak at 528 nm) of the QD-

PDI system; χ_{PDI} and χ_{QD} are the excitation spectra of the PDI and QD, respectively (normalized to the PDI peak at 528 nm). In the measurement of excitation spectra, the emission was fixed at 620 nm where only PDI emission is detected. The excitation spectrum feature below 400 nm for the composite sample indicates that there is energy transfer from the QD to the PDI (Figure S3). The value of χ_{PDI} was obtained from the excitation spectra of PDI-only sample in same PDI concentration as in the QD-PDI sample. The value of χ_{QD} was calculated by the excitation spectra of QD-PDI sample minus the excitation spectra of PDI-only sample. The values of E_{FRET} are listed in Table 2. The values of E_{FRET} for the PDI-C5-COOH-, PDI-C11-COOH-, PDI-C4-NH_2-, PDI-C12-NH_2-based composites were 82.2%, 91.0%, 25.3%, and 25.5%, respectively, at the highest loadings. At similar PDI anchoring ratios, E_{FRET} for the QD-PDI-C5-COOH composite was 49.7% at 1:16 molar ratio while the QD-PDI-C11-COOH composite only yielded 15.2% at 1:17 molar ratio. Similarly, E_{FRET} for the QD-PDI-C4-NH_2 composites was 17.2% at 1:20 molar ratio while that for the QD-PDI-C12-NH_2 composite was only 8.6% at 1:19 molar ratio. The lower values of E_{FRET} for the longer alkyl chain PDI is again evidence for distance dependent energy transfer.

Table 2. The FRET efficiency E_{FRET} and photoluminescence quantum yield (Φ_{PL}) of QD-PDI system for different ratios of *bound* PDI molecules. The FRET efficiency was calculated from excitation spectra of the emission at 620 nm. The Φ_{PL} value for the QD-PDI samples is obtained from the total emission (QD + PDI) of the system.

QD-PDI-C5-COOH			QD-PDI-C11-COOH			QD-PDI-C4-NH_2			QD-PDI-C12-NH_2		
[QD]: [PDI]	E_{FRET} (%)	Φ_{PL} (%)	[QD]: [PDI]	E_{FRET} (%)	Φ_{PL} (%)	[QD]: [PDI]	E_{FRET} (%)	Φ_{PL} (%)	[QD]: [PDI]	E_{FRET} (%)	Φ_{PL} (%)
1:0	0	45	1:0	0	45	1:0	0	45	1:0	0	45
1:3	10.6	33	1:4	9.2	29	1:0.4	0.5	28	1:1	2.9	32
1:5	17.7	28	1:6	11.4	28	1:1	1.0	30	1:3	4.4	31
1:6	24.2	27	1:10	13.8	29	1:2	3.0	25	1:8	5.7	29
1:8	28.8	28	1:17	15.2	35	1:4	4.1	20	1:10	7.5	28
1:16	49.7	28	1:42	25.0	40	1:7	6.5	22	1:19	8.6	35
1:53	58.7	33	1:88	63.2	51	1:20	17.2	24	1:35	11.9	42
1:81	82.2	31	1:138	91.0	57	1:30	25.3	23	1:53	25.5	50

While the QD PL intensity decreased with PDI loading, the PDI emission itself was enhanced, as expected for FRET (Figure S5). For example, in QD-PDI-C11-COOH nanocrystals, the PDI-C11-COOH emission was enhanced at low loading ratios (1:3 to 1:17) as energy migrated from QDs but then the PL intensity subsequently decreased as more PDIs were adsorbed to the QD surface (1:42 to 1:138) (Figure S5b). At a molar ratio of 1:138, the composite exhibited a PL spectrum resembling that of aggregated PDI.[22] Since the absorption spectrum of the PDI ligand on its own and that of the

QD-PDI composite are nearly identical, the emission likely originated from excimers (Figure S6). Hence despite the steric protection, the surface bound PDI molecules showed electronic interaction with each other particularly in their excited state.

Before discussing the Φ_{PL} values, it is important to note that these values were obtained by absolute quantum yield method using an integrating sphere. This meant all Φ_{PL} values included the total emission of the entire sample measured. Compared to the as-synthesized QDs, the Φ_{PL} was enhanced from 45% (as-synthesized QDs) to 57% (QD-PDI-C11-COOH system) at the molar ratio of 1:138 in the composite as measured in an integrating sphere under 365 nm excitation (Table 2). Although the PDI monomer has near unity Φ_{PL}, the PDI aggregates have lower Φ_{PL}.[29] This explains the lower 57% Φ_{PL} value that was measured despite the very high FRET efficiency. For QD-PDI-C5-COOH composites, the PL intensity of the PDI likewise increased at low loading ratios then decreased at high loading ratios (Figure S5a). This can be attributed to 3 effects: 1. poorer surface passivation of the QDs; 2. less efficient FRET; and 3. lower Φ_{PL} of PDI aggregates. Again, there is clear evidence for PDI aggregates in the red-shifted and broadened emission spectra. The QD-PDI-C5-COOH sample showed broader emission and hence greater PDI aggregation than the QD-PDI-C11-COOH sample at a similar donor-acceptor ratio. Due to the shorter alkyl chain of PDI-C5-COOH, the distance between PDIs on the QD surface was expected to be closer than for QD-PDI-C11-COOH. The Φ_{PL} of the QD-PDI-C5-COOH composite was only 31% at a molar ratio of 1:81 compared to 51% for the QD-PDI-C11-COOH composite at a ratio of 1:88 (Table 2). Similar observations were recorded for the amine functionalized PDI-based composites. It should be noted that energy migration between PDI molecules on the QD surface is possible at the localized concentration on the QD surface.[30] Indeed, our group investigated energy migration in PDI materials previously[29, 31-32] and we employed our experience to design the PDI molecules in this study.

Excited state lifetimes of the QD and QD-PDI composite samples were measured using time-correlated single photon counting (TCSPC, see Supporting information for details, Figure 4). While the actual excited state decay mechanisms can be complex in these systems, the decay data could be fitted to a bi-exponential model with the average lifetime calculated to be 13.3 ns for the QD-only sample. The average lifetimes of the QD emission of the QD-PDI-C5-COOH (1:81), QD-PDI-C11-COOH (1:138), QD-PDI-C4-NH_2 (1:30), and QD-PDI-C12-NH_2 (1:53), samples were 1.4 ns, 2.3 ns, 2.0 ns, and 3.9 ns, respectively (Table S2). The strong reduction in lifetime is attributed to FRET from the QDs to the PDIs. It is noteworthy that the PL excited state lifetime quenching (Figure 4b) and the PL intensity quenching (Figure S4) showed similar qualitative trends.

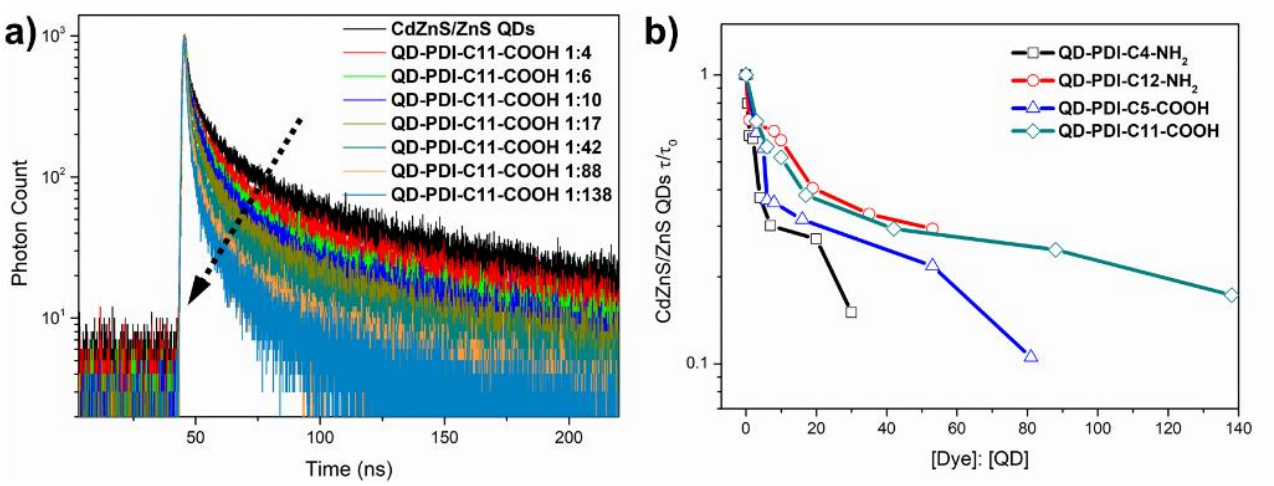

Figure 4. Time-resolved PL spectra of QDs in QD-PDI composites with different PDI loading ratios, a) PDI-C4-NH_2, b) The QDs lifetime quenching ratio in four QD-PDI composites with different dye to QDs molar ratios ([Dye]: [QD]). QDs emission was detected at 471 nm. τ_0 was the fluorescent lifetime of QDs at 417 nm with the absence of PDIs, and τ was the fluorescent lifetime of QDs at 471 nm with the presence of PDIs.

In Figures 5a and 5b, we plot the FRET efficiency for the 4 dyes using the reduction in lifetimes determined by TCSPC. Firstly, we observe that there is indeed a sharp rise in PL quenching when the number of dye molecules is in the regime $0 < \lambda < 1$. Typically, 20-40% PL quenching is observed which is consistent with very efficient FRET based quenching. However, for larger ratios of λ, the efficiency tails off rapidly and only climbs very slowly for $\lambda >> 1$. Even when tens of PDI molecules are adsorbed, quenching does not rise beyond 70%. To rationalize this, we must assume that although 1 or 2 single PDI molecules can act as efficient quenchers, there is a very high degree of aggregation as soon as multiple dyes are adsorbed. Furthermore, these aggregates are more or less unable to quench. We now attempt to employ a basic statistical model to explain the experimental trends, based on an approach used by Funston et al. and Beane et al.[33-35], which is in turn adopted from Mattousi's work[36-37].

For a QD under low photoexcitation rates, we assume classical kinetics and that each dye molecule acts independently and has the same probability of harvesting excitons through energy transfer. Then the rate of energy transfer for n independent dye molecules is given by:

$$E(n) = \frac{n}{n+\left[\frac{R}{R_O}\right]^6} \qquad (5)$$

where R/ R_o is the mean separation of the quencher relative to the Forster radius, R_o. The probability that any given QD has n quenchers if the mean ratio of adsorbed quenchers to QDs is λ, is given by

$$P(n) = \frac{e^{-\lambda}\lambda^n}{n!} \qquad (6)$$

And hence the observed quenching efficiency is given by the sum over the Poisson distribution:

$$E = \sum_{n=0}^{n=\infty} E(n)P(n) = \sum_{n=0}^{n=\infty} \frac{n}{n+\left[\frac{R}{R_o}\right]^6} \frac{e^{-\lambda}\lambda^n}{n!} \qquad (7)$$

Here R_o = 4.1 nm is the Förster radius from equation 1 and the FRET efficiency is determined experimentally from Table S2. The functionalized PDI molecules range in separation from the surface from R ~ 1.1 nm to R~ 2.4nm, corresponding to R/R_o ~0.3 to 0.6, which means that the dyes are well within the range expected for efficient FRET. Note that equation 5 predicts that even 1 or 2 quencher molecules are sufficient to quench the QD PL if $R< R_o$. Hence, we conclude from Table 2 that the vast majority of dye molecules are inactive, although for $\lambda < 2$, we do see strong quenching. The assumption that each dye molecule behaves independently and identically is a simplification. As we add more dyes, surface segregation reduces FRET efficiency. Indeed, the broadening emission spectra demonstrate that AIQ occurs at high coverages, due to preferential surface assembly of the PDI dyes.

Previous work by Funston et al. established that in favourable cases, complete quenching can be achieved for λ ~1.[35] We conclude that a mechanism to preclude surface aggregation is essential to obtain quantitative and sustained energy transfer. To try and get an estimate for the degree of aggregation of the dyes, we make the following further assumptions to modify eq.7.

a. We assume all acceptors lie at the same fixed distance from the surface. This value is obtained from the fitting process.
b. We assume that single acceptor molecules are active FRET quenchers but that all aggregates from dimer upwards are non-quenching.
c. We assume the concentration of adsorbed single quenchers is controlled by a surface equilibrium constant K for values of n >= 1.

Hence,

If n = 1, $$E(1) = \frac{1}{1+\left[\frac{R}{R_o}\right]^6} \frac{e^{-\lambda}\lambda^n}{n!} \qquad (8a)$$

If n > 1, $$\mathrm{E}(n) = \frac{K*n}{K*n+\left[\frac{R}{R_o}\right]^6} \frac{e^{-\lambda}\lambda^n}{n!} \qquad (8b)$$

The value of K represents a surface solubility constant. Small values equate to only a small fraction of the adsorbed acceptor molecules being isolated and hence active. In Figure 5, we present some fits using R/R_o = 0.40 and R/R_o = 0.45 for the shorter derivatives and R/R_o = 0.55 and R/R_o = 0.60 for the longer derivatives. These reproduce the trends well provided that K is very small, consistent with

virtually quantitative aggregation of all PDI acceptor molecules on the surface. The smaller value of K for the shorter chain PDI quenchers suggests they aggregate more strongly than the longer chain derivatives.

The model predicts the high rate of quenching observed experimentally for $\lambda < 1$ and then the rapid decrease in the quenching efficiency. The peak in efficiency is due to the fact that maximum quenching occurs for QDs coated with a single PDI molecule. As more acceptors are added, they dimerize, i.e. aggregate and become non-quenchers. Because of the low value of the equilibrium constant, K, there is a very small increase in the mean numbers of active quenchers, even for high values of λ.

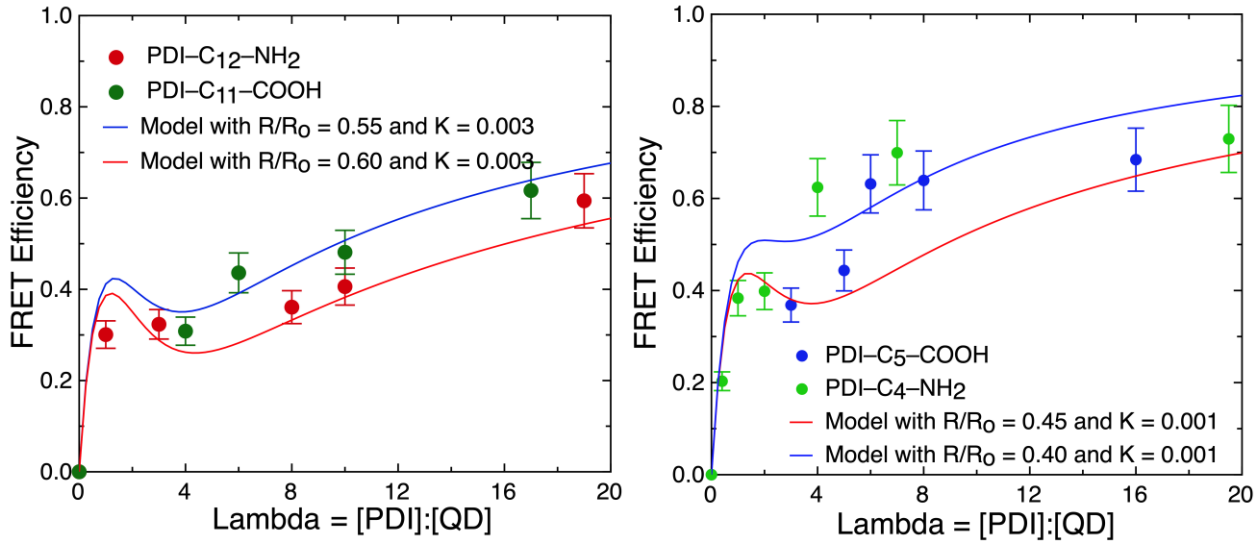

Figure 5: Quenching of CdSe@ZnS QDs by 4 different PDI quencher molecules as a function of the ratio λ = [PDI]:[QD]. (Left) Data for the two longer chain derivatives, PDI-C_{11}-COOH and PDI-C_{12}-NH_2. Also shown are two representative fits using equation 5 with R/R_o being set to 0.55 or 0.60 with the surface dissociation constant K = 0.003. (Right) Data for the two shorter chain derivatives, PDI-C_5-COOH and PDI-C_4-NH_2. Also shown are two representative fits using equation 5 with the value of R/R_o being set to 0.45 or 0.40 and with the surface dissociation constant K = 0.001. FRET efficiency values based on the reduction in donor lifetime are taken from Table S2.

QD-PDI composite colloidal stability study

Changes in both the QD PL (at 471nm) and PDI PL (at 538nm) occurred because of ageing of the hybrid nanocrystals and the results are shown in Figure 6. In the case of QD-PDI-C5-COOH, the PL emission of both the QD and PDI-C5-COOH were strongly quenched over 48 h (Figure 6a, Figure S7a). The PL quenching was quite fast in the first 5 h with the QD and PDI PL intensities dropping to 71% and 28% of the original values, respectively. After 24 h, there were further small decreases to 68% and 25% of the original PL intensity, and the composites still exhibited 67% and 23% QD and PDI PL intensity after total 48 h storage. We believe this loss of PL is due to slow desorption of the

PDI from the surface. This led to lower PDI PL intensity but also created surface vacancies and increased non-radiative losses in the QDs. Increased light scattering was evident in the absorbance spectra due to aggregated QDs after 48 h storage (Figure S7c). In the case of QD-PDI-C11-COOH, the PL intensity of PDI-C11-COOH declined slowly over the full 48 h period, which was consistent with its stronger binding. In fact, the QD PL intensity was firstly enhanced to 122% of the initial value in the first 0.5 h due to a reduction in FRET and it still exhibited 104% PL intensity (relative to the initial value) after 48 h storage (Figure 6d). There was only very slight light scattering evident in these QD-PDI-C11-COOH composite nanocrystals due to the lower rate of aggregation (Figure S7d).

As expected, the amine functionalized PDIs were less stable upon storage. At longer times, serious light scattering indicated the formation of QD aggregates (Figure S7e). Similarly, the desorption of PDI-C12-NH_2 led to the loss of both QD and PDI-C12-NH_2 PL (Figure 4b). The QD-PDI-C12-NH_2 nanocrystals exhibited slower PL quenching rate than the QD-PDI-C4-NH_2 nanocrystals. In general, there was more light scattering evident in the aged amine-capped nanocrystals compared to carboxylic acid-based ones (Figure S7). The fact that PDI desorption also resulted in QD PL decreases strongly suggests that the anchor group also serves to passivate surface traps.

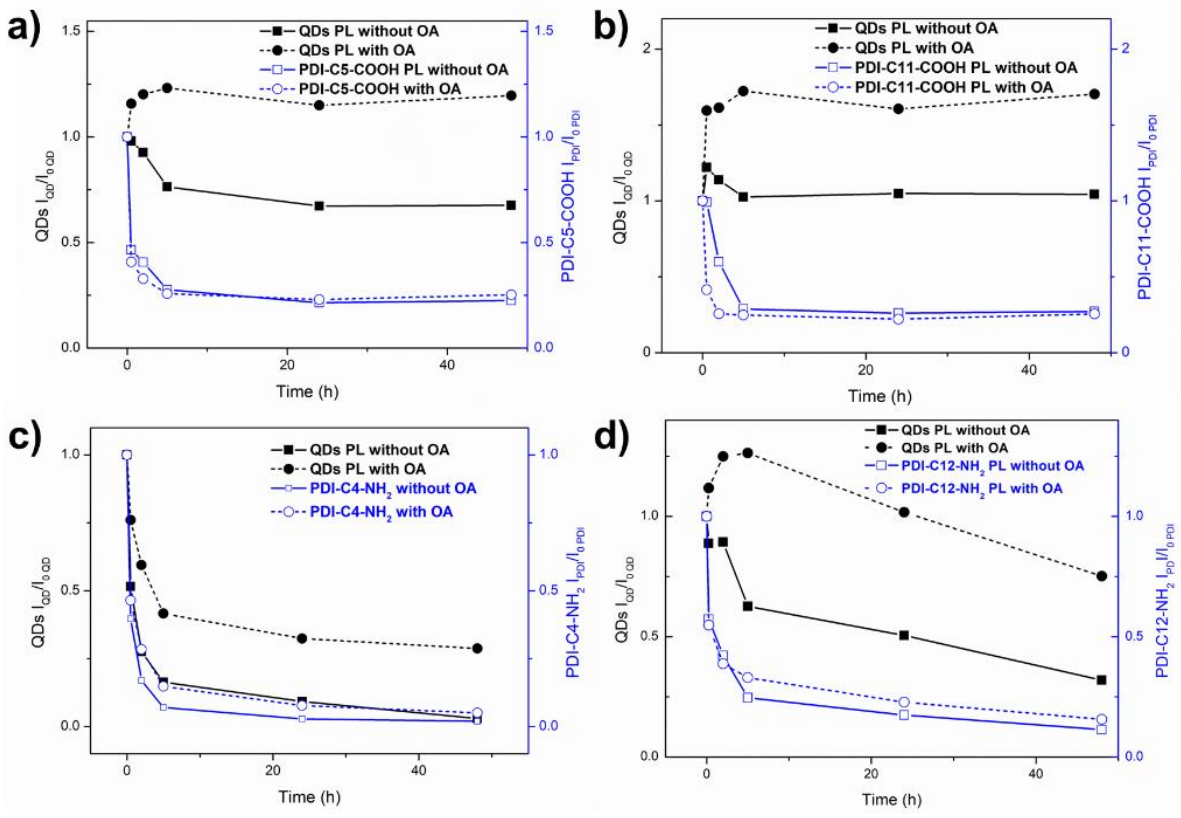

Figure 6. The PL intensity change trend of QDs (471 nm) and PDIs (538 nm) in QD-PDI composites with the absence and presence of oleic acid in 48 h. a) PDI-C5-COOH, b) PDI-C11-COOH, c) PDI-C4-NH_2, and d) PDI-C12-NH_2. Black

curves are QDs change (square without oleic acid, circle with oleic acid), blue curves are PDI-based organic dyes (square without oleic acid, circle with oleic acid). All samples were excited at 365 nm. $I_{0\,QD}$ and $I_{0\,PDI}$ were the PL intensity of QDs and PDIs in fresh composite solution at 471 nm and 538 nm, respectively. I_{QD} and I_{PDI} were the PL intensity of QDs and PDIs within 48 h at 471 nm and 538 nm, respectively.

An important question is whether there is a competitive equilibrium established between adsorbed PDI and oleate ligands. To probe the reversibility of the exchange between PDIs and oleate ligands, oleic acid was added into fresh, purified QD-PDI composites at the same fixed concentration of PDI. The absorbance and PL spectra were also examined after 48 h storage in air at room temperature. The rate of PL loss due to PDI desorption was similar both in the presence and absence of oleic acid. After 48 h storage, the PL intensity of PDIs in the presence of the nanocrystals was quite close to that of pure PDIs solution under same concentration, which indicated the total desorption of PDIs. The QD-PDI-C5-COOH- and QD-PDI-C11-COOH-based samples exhibited enhanced QD PL which were up to 120% and 170% of the initial value, respectively, with the passivation by oleate in composites (Figure 6a, b). Similarly, the PDI-C4-NH_2-based composite exhibited slower quenching of QD PL with the oleate passivation, retaining 29% PL intensity after 48 h (Figure 6c, Figure S7e). In addition, light scattering was also eliminated indicating reduced QD aggregation in the presence of added oleic acid (Figure S7e). In the QD-PDI-C12-NH_2 composite, QD PL intensity increased in the first 5 h again because of QD surface passivation by oleate (Figure 6d). After 48 h storage, there was still 75% PL intensity left. The loss of PL was significantly slowed down by the addition of oleic acid.

Oleic acid was also added into 48 h aged QD-PDI composites solution and similar QD PL intensity enhancement was observed. This suggests the reversibility of the exchange between functionalized PDIs and oleate without the alteration of QD surface metal atoms.[17, 20] In addition, the strong binding of carboxylic acid group and longer alkyl chain improved the colloidal stability of QDs in composites with slower PDI desorption.

Conclusions

Energy transfer between QDs and adsorbed dyes have been studied in four $Cd_xZn_{1-x}S$/ZnS-PDI hybrid nanocrystals. The four PDI derivatives exhibited different adsorption affinities and energy transfer efficiencies. The longer alkyl chain derivatives afforded overall higher Φ_{PL} composites due to lower PDI aggregation despite slightly lower intrinsic FRET efficiency. The carboxylic acid groups enabled better PDI binding to the QDs resulting in higher surface ligand coverage compared to the amine anchor groups. Using more than one anchoring group per dye molecule may improve dye binding.[38] Minimizing surface aggregation of the dyes is a critical factor that controls energy transfer and

photoluminescence efficiency. Inclusion of an emissive energy trap may be a solution towards unity photoluminescence efficiency.[32]

Supporting Information

Supporting Information file contains detailed synthesis procedures for QDs and PDIs, determination of molar extinction coefficient for QDs, additional photophysical characterization of QD-PDI composites, and QD-PDI composite stability data. This is available free of charge on the ACS Publications website.

Acknowledgements

This work was supported by the ARC Centre of Excellence in Exciton Science (CE170100026). The authors acknowledge access to the Mass Spectrometry and Proteomics Facility (MSPF) at the Bio21 Institute, University of Melbourne.

References

1. Klajn, R.; Stoddart, J. F.; Grzybowski, B. A., Nanoparticles Functionalised with Reversible Molecular and Supramolecular Switches. *Chem. Soc. Rev.* **2010**, *39*, 2203-2237.
2. Freeman, R.; Willner, I., Optical Molecular Sensing with Semiconductor Quantum Dots. *Chem. Soc. Rev.* **2012**, *41*, 4067-4085.
3. Silvi, S.; Credi, A., Luminescent Sensors Based on Quantum Dot–Molecule Conjugates. *Chem. Soc. Rev.* **2015**, *44*, 4275-4289.
4. Lim, S. J.; Ma, L.; Schleife, A.; Smith, A. M., Quantum Dot Surface Engineering: Toward Inert Fluorophores with Compact Size and Bright, Stable Emission. *Coord. Chem. Rev.* **2016**, *320-321*, 216-237.
5. Wu, P.; Yan, X.-P., Doped Quantum Dots for Chemo/Biosensing and Bioimaging. *Chem. Soc. Rev.* **2013**, *42*, 5489-5521.
6. Hildebrandt, N.; Spillmann, C. M.; Algar, W. R.; Pons, T.; Stewart, M. H.; Oh, E.; Susumu, K.; Díaz, S. A.; Delehanty, J. B.; Medintz, I. L., Energy Transfer with Semiconductor Quantum Dot Bioconjugates: A Versatile Platform for Biosensing, Energy Harvesting, and Other Developing Applications. *Chem. Rev.* **2017**, *117*, 536-711.
7. Martynenko, I. V.; Litvin, A. P.; Purcell-Milton, F.; Baranov, A. V.; Fedorov, A. V.; Gun'ko, Y. K., Application of Semiconductor Quantum Dots in Bioimaging and Biosensing. *J. Mater. Chem. B* **2017**, *5*, 6701-6727.
8. Litvin, A. P.; Martynenko, I. V.; Purcell-Milton, F.; Baranov, A. V.; Fedorov, A. V.; Gun'ko, Y. K., Colloidal Quantum Dots for Optoelectronics. *J. Mater. Chem. A* **2017**, *5*, 13252-13275.
9. Chern, M.; Kays, J. C.; Bhuckory, S.; Dennis, A. M., Sensing with Photoluminescent Semiconductor Quantum Dots. *Methods Appl. Fluores.* **2019**, *7*, 012005.
10. Coe, S.; Woo, W.-K.; Bawendi, M.; Bulović, V., Electroluminescence from Single Monolayers of Nanocrystals in Molecular Organic Devices. *Nature* **2002**, *420*, 800-803.
11. Huynh, W. U.; Dittmer, J. J.; Alivisatos, A. P., Hybrid Nanorod-Polymer Solar Cells. *Science* **2002**, *295*, 2425-2427.
12. Medintz, I. L.; Clapp, A. R.; Mattoussi, H.; Goldman, E. R.; Fisher, B.; Mauro, J. M., Self-assembled Nanoscale Biosensors Based on Quantum Dot FRET Donors. *Nat. Mater.* **2003**, *2*, 630-638.
13. Zhang, Q.; Atay, T.; Tischler, J. R.; Bradley, M. S.; Bulović, V.; Nurmikko, A. V., Highly Efficient Resonant Coupling of Optical Excitations in Hybrid Organic/Inorganic Semiconductor Nanostructures. *Nat. Nanotech.* **2007**, *2*, 555-559.
14. Cardoso Dos Santos, M.; Algar, W. R.; Medintz, I. L.; Hildebrandt, N., Quantum dots for Förster Resonance Energy Transfer (FRET). *TrAC, Trends Anal. Chem.* **2020**, *125*, 115819.
15. Hildebrandt, N., How to Apply FRET: From Experimental Design to Data Analysis. In *FRET – Förster Resonance Energy Transfer*, Medintz, I. L.; Hildebrandt, N., Eds. Wiley-VCH: 2014; pp 105-163.
16. Tsai, H.-Y.; Kim, H.; Massey, M.; Krause, K. D.; Algar, W. R., Concentric FRET: A Review of the Emerging Concept, Theory, and Applications. *Methods Appl. Fluores.* **2019**, *7*, 042001.
17. Liu, M.; Wang, Y.-Y.; Liu, Y.; Jiang, F.-L., Thermodynamic Implications of the Ligand Exchange with Alkylamines on the Surface of CdSe Quantum Dots: The Importance of Ligand–Ligand Interactions. *J. Phys. Chem. C* **2020**, *124*, 4613-4625.
18. Hassinen, A.; Moreels, I.; de Mello Donegá, C.; Martins, J. C.; Hens, Z., Nuclear Magnetic Resonance Spectroscopy Demonstrating Dynamic Stabilization of CdSe Quantum Dots by Alkylamines. *J. Phys. Chem. Lett.* **2010**, *1*, 2577-2581.
19. Hens, Z.; Martins, J. C., A Solution NMR Toolbox for Characterizing the Surface Chemistry of Colloidal Nanocrystals. *Chem. Mater.* **2013**, *25*, 1211-1221.
20. Knauf, R. R.; Lennox, J. C.; Dempsey, J. L., Quantifying Ligand Exchange Reactions at CdSe

Nanocrystal Surfaces. *Chem. Mater.* **2016**, *28*, 4762-4770.
21. Fritzinger, B.; Moreels, I.; Lommens, P.; Koole, R.; Hens, Z.; Martins, J. C., In Situ Observation of Rapid Ligand Exchange in Colloidal Nanocrystal Suspensions Using Transfer NOE Nuclear Magnetic Resonance Spectroscopy. *J. Am. Chem. Soc.* **2009**, *131*, 3024-3032.
22. Moreels, I.; Justo, Y.; De Geyter, B.; Haustraete, K.; Martins, J. C.; Hens, Z., Size-Tunable, Bright, and Stable PbS Quantum Dots: A Surface Chemistry Study. *ACS Nano* **2011**, *5*, 2004-2012.
23. Coppel, Y.; Spataro, G.; Pagès, C.; Chaudret, B.; Maisonnat, A.; Kahn, M. L., Full Characterization of Colloidal Solutions of Long-Alkyl-Chain-Amine-Stabilized ZnO Nanoparticles by NMR Spectroscopy: Surface State, Equilibria, and Affinity. *Chem. Eur. J.* **2012**, *18*, 5384-5393.
24. Dworak, L.; Matylitsky, V. V.; Ren, T.; Basché, T.; Wachtveitl, J., Acceptor Concentration Dependence of Förster Resonance Energy Transfer Dynamics in Dye–Quantum Dot Complexes. *J. Phys. Chem. C* **2014**, *118*, 4396-4402.
25. Li, X.; Nichols, V. M.; Zhou, D.; Lim, C.; Pau, G. S. H.; Bardeen, C. J.; Tang, M. L., Observation of Multiple, Identical Binding Sites in the Exchange of Carboxylic Acid Ligands with CdS Nanocrystals. *Nano Lett.* **2014**, *14*, 3382-3387.
26. Li, X.; Slyker, L. W.; Nichols, V. M.; Pau, G. S. H.; Bardeen, C. J.; Tang, M. L., Ligand Binding to Distinct Sites on Nanocrystals Affecting Energy and Charge Transfer. *J. Phys. Chem. Lett.* **2015**, *6*, 1709-1713.
27. Lee, K.-H.; Lee, J.-H.; Song, W.-S.; Ko, H.; Lee, C.; Lee, J.-H.; Yang, H., Highly Efficient, Color-Pure, Color-Stable Blue Quantum Dot Light-Emitting Devices. *ACS Nano* **2013**, *7*, 7295-7302.
28. Bae, W. K.; Nam, M. K.; Char, K.; Lee, S., Gram-Scale One-Pot Synthesis of Highly Luminescent Blue Emitting Cd1−xZnxS/ZnS Nanocrystals. *Chem. Mater.* **2008**, *20*, 5307-5313.
29. Zhang, B.; Soleimaninejad, H.; Jones, D. J.; White, J. M.; Ghiggino, K. P.; Smith, T. A.; Wong, W. W. H., Highly Fluorescent Molecularly Insulated Perylene Diimides: Effect of Concentration on Photophysical Properties. *Chem. Mater.* **2017**, *29*, 8395-8403.
30. Chen, C.; Corry, B.; Huang, L.; Hildebrandt, N., FRET-Modulated Multihybrid Nanoparticles for Brightness-Equalized Single-Wavelength Barcoding. *J. Am. Chem. Soc.* **2019**, *141*, 11123-11141.
31. Banal, J. L., et al., Energy Migration in Organic Solar Concentrators with a Molecularly Insulated Perylene Diimide. *J. Phys. Chem. C* **2016**, *120*, 12952-12958.
32. Zhang, B., et al., FRET-Enhanced Photoluminescence of Perylene Diimides by Combining Molecular Aggregation and Insulation. *J. Mater. Chem. C* **2020**, *8*, 8953-8961.
33. Beane, G.; Boldt, K.; Kirkwood, N.; Mulvaney, P., Energy Transfer between Quantum Dots and Conjugated Dye Molecules. *J. Phys. Chem. C* **2014**, *118*, 18079-18086.
34. Beane, G. A.; Morfa, A. J.; Funston, A. M.; Mulvaney, P., Defect-Mediated Energy Transfer between ZnO Nanocrystals and a Conjugated Dye. *J. Phys. Chem. C* **2012**, *116*, 3305-3310.
35. Funston, A. M.; Jasieniak, J. J.; Mulvaney, P., Complete Quenching of CdSe Nanocrystal Photoluminescence by Single Dye Molecules. *Adv. Mater.* **2008**, *20*, 4274-4280.
36. Clapp, A. R.; Medintz, I. L.; Mattoussi, H., Förster Resonance Energy Transfer Investigations Using Quantum-Dot Fluorophores. *ChemPhysChem* **2006**, *7*, 47-57.
37. Clapp, A. R.; Medintz, I. L.; Mauro, J. M.; Fisher, B. R.; Bawendi, M. G.; Mattoussi, H., Fluorescence Resonance Energy Transfer Between Quantum Dot Donors and Dye-Labeled Protein Acceptors. *J. Am. Chem. Soc.* **2004**, *126*, 301-310.
38. Ren, T.; Mandal, P. K.; Erker, W.; Liu, Z.; Avlasevich, Y.; Puhl, L.; Müllen, K.; Basché, T., A Simple and Versatile Route to Stable Quantum Dot−Dye Hybrids in Nonaqueous and Aqueous Solutions. *J. Am. Chem. Soc.* **2008**, *130*, 17242-17243.

TOC Graphic